Research Article

BIOMEDICAL Journal of Scientific & Technical Research

ISSN: 2574 -1241

DOI: 10.26717/BJSTR.2020.29.004798

# $^{19}$F-Magnetic Resonance Imaging for Tracking Bone-Marrow Macrophages in a Model of Experimental Autoimmune Myocarditis: A Pilot Study

**Christine Gonzales[1#], Hikari AI Yoshihara[1#], Ruud B van Heeswijk[2,9], Pascal Mieville[3], Lothar Helm[3], Przemyslaw Blyszczuk[4,5], Gabriela Kania[6], Urs Eriksson[4,7] and Juerg Schwitter[1,8*]**

[1]*Division of Cardiology, Lausanne University Hospital (CHUV), Lausanne, Switzerland*

[2]*Cardiovascular Magnetic Resonance, Department of Radiology, University of Lausanne (UNIL) and Lausanne University Hospital (CHUV), Lausanne, Switzerland*

[3]*Institut des Sciences et IngénierieChimiques, Ecole Polytechnique Fédérale de Lausanne (EPFL), Lausanne, Switzerland*

[4]*Cardioimmunology, Cardiovascular Research, Institute of Physiology, University of Zurich, Switzerland.*

[5]*Department of Clinical Immunology, Jagiellonian University Medical College, Cracow, Poland*

[6]*Center of Experimental Rheumatology, Department of Rheumatology, University Hospital Zurich, Switzerland*

[7]*Department of Medicine, Zurich Regional Health Centre (GZO), Wetzikon, Switzerland*

[8]*Cardiac Magnetic Resonance Center, Lausanne University Hospital (CHUV), Lausanne, Switzerland*

[9]*Center for BioMedical Imaging (CIBM), Lausanne and Geneva, Switzerland*

[#]*Both authors contributed equally to this manuscript.*

***Corresponding author:** Juerg Schwitter, Division of Cardiology, Lausanne University Hospital (CHUV); Cardiac Magnetic Resonance Center, Lausanne University Hospital (CHUV), Lausanne, Switzerland

ARTICLE INFO

Received: July 28, 2020

Published: August 07, 2020

**Citation:** Christine Gonzales, Hikari AI Yoshihara, Ruud B van Heeswijk, Pascal Mieville, Lothar Helm, Przemyslaw Blyszczuk, Gabriela Kania, Urs Eriksson, Juerg Schwitter. $^{19}$F-Magnetic Resonance Imaging for Tracking Bone-Marrow Macrophages in a Model of Experimental Autoimmune Myocarditis: A Pilot Study. Biomed J Sci & Tech Res 29(3)-2020. BJSTR. MS.ID.004798.

**Keywords:** Experimental Autoimmune Myocarditis; Bone-Marrow Macrophage; Perfluorocarbon; $^{19}$F-MRI; $^{19}$F-NMR

ABSTRACT

**Object:** Fluorine-19 ($^{19}$F)-MRI can detect specific cell subsets *in-vivo*, and infused perfluorocarbon label accumulates in myocardial macrophages in mice with Experimental Autoimmune Myocarditis (EAM). However, the extent of myocardial migration by labeled macrophages versus uptake by resident macrophages is unknown. Here, we tested the feasibility of tracking by $^{19}$F-MRI of *in-vitro* labeled bone-marrow-derived macrophages (BMM) after their adoptive transfer.

**Materials and Methods:** BMM from CD45.1 mice were $^{19}$F-labeled *in-vitro* with CS-1000 and were then intravenously injected (1-14 × $10^6$ cells) into CD45.2 BALB/c mice with EAM. *In-vivo* $^{19}$F-MRI (9.4T) was performed 2 days later, and $^{19}$F content of organ extracts was determined by $^{19}$F-NMR spectroscopy, with BMM migration characterized by immunohistochemistry and flow cytometry.

**Results:** Labeling yielded 1.02 ± 0.50 × $10^{13}$ $^{19}$F-atoms/cell, and a variable *in-vivo* $^{19}$F-MRI signal was detected in the liver, lungs, and spleen. A faint $^{19}$F signal was detectable in some isolated hearts, and the CD45.1 marker was present in a minor fraction of inflammatory cells. *Ex-vivo* $^{19}$F-NMR, immunohistochemistry, and flow cytometry confirmed these *in-vivo* measurements.

**Discussion:** $^{19}$F-MRI-based cell tracking in the EAM model demonstrates accumulation of intravenously-injected labeled BMM primarily in the liver, spleen, and lungs, with minimal accumulation in the inflamed myocardium.

**Abbreviations:** $^{19}$F: Fluorine-19; ANOVA: Analysis of Variance; BMM: Bone-Marrow Macrophages; EAM: Experimental Autoimmune Myocarditis; FBS: Fetal Bovine Serum; IV: Intravenous; PFC: Perfluorocarbon; MRI: Magnetic Resonance Imaging; MRS: Magnetic Resonance Spectroscopy; NMR: Nuclear Magnetic Resonance; OCT: Optimal Cutting Temperature; PBS: Phosphate Buffered Saline; RPMI: Roswell Park Memorial Institute; SPECT: Single-Photon Emission Computed Tomography; SPGR: Spoiled-Gradient Echo; SSFP: Steady State at Free Precession; T: Tesla; TE: Echo Time; TR: Repetition Time; TFA: Trifluoroacetic Acid

## Introduction

In recent years, $^{19}$F-MRI has emerged as an attractive method to detect perfluoro-carbon (PFC) compounds non-invasively in animal experiments [1,2]. Because $^{19}$F background signal is effectively absent in animals and humans, $^{19}$F-MRI can unequivocally detect an exogenous $^{19}$F compound with high specificity of the signal. As the signal received by an MR volume coil with a homogenous $B_1$ field is directly proportional to the amount of $^{19}$F nuclei present in the tissue under experimental conditions allowing uniform nuclear spin relaxation and excitation, the signal can be related to a reference of known concentration, rendering this technique quantitative [3,4]. Moreover, unlike molecular imaging methods based upon positron emission or hyperpolarized carbon-13, non-volatile PFC compounds are not limited by signal decay over time, and the time window for their detection can therefore last several days. Finally, $^{19}$F-MRI images can be merged with conventional $^{1}$H-MRI images to match the $^{19}$F signal with its exact anatomic location in the body and to also correlate it with function or other tissue characteristics.

Accordingly, $^{19}$F-MRI has been used successfully to detect and track well-defined cell populations in rodent models of inflammation, including myocardial infarction [5-7], cerebral ischemia [6], pneumonia [8], atherosclerosis [9], arthritis [10], and tumors infiltrated by macrophages [11]. In a recent study, we successfully visualized heart-infiltrating macrophages *in-vivo* by $^{19}$F-MRI in a model of experimental autoimmune myocarditis (EAM) after IV injection of a PFC emulsion [12]. The EAM model is a $CD4^+$ T cell-mediated disease which closely resembles the phenotype of human myocarditis, including its progression toward inflammatory dilated cardiomyopathy [13]. Inflammatory cardiomyopathy, on the other hand, is an important cause of heart failure in young patients and its prevalence is most likely largely underestimated [14]. Cardiac inflammation in EAM typically peaks approximately 21 days after immunization, as assessed by hematoxylin and eosin histological staining of inflammatory infiltrates, followed by a transition to diffuse interstitial fibrosis and end-stage heart failure [15].

Our earlier study demonstrated by immunohistochemistry and flow cytometry the presence of PFC in macrophages within the inflamed myocardium [12]. However, the precise origin of these PFC-labeled macrophages remains unknown since the IV-injected PFC can be taken up by either circulating monocytes or by macrophages which differentiate from heart-infiltrating or resident immature precursor cells in the inflamed myocardium. Several lines of evidence suggest an immunosuppressive role of myeloid cells and macrophages in regulating disease severity and outcome in myocarditis [16,17]. If circulating cells are responsible for a major part of cardiac infiltrates detected by $^{19}$F-MRI in the EAM model, it should then be possible in principle to follow the migration of labeled monocytes or macrophages to the inflamed myocardium.

Recent reports have demonstrated that T cells, splenocytes, stem cells, and endothelial cells can be labeled with PFC *in-vitro* and then re-injected to be tracked by $^{19}$F-MRI [4,18-22]. The aim of this study was to determine the feasibility of using this method to track macrophage migration in the EAM model as a proof-of-concept. Bone-marrow-derived macrophages (BMM) were labeled with PFC *in-vitro* and re-injected into EAM mice in the early phase of inflammation, before the peak, for cell tracking by $^{19}$F-MRI. $^{19}$F-MRI was performed on the heart as well as the lungs, spleen and liver to best characterize the fate of the injected PFC-labeled BMM, and the results were confirmed with *ex-vivo* $^{19}$F-NMR spectroscopy, immunohistochemistry, and flow cytometry experiments.

## Materials and Methods

### Animals

Mice were maintained under specific pathogen-free conditions. EAM was induced in 52 male BALB/c (CD45.2) mice by subcutaneous injections of αMyHC peptide (alpha myosin heavy chain, Ac-RSLKLMATLFSTYASADROH; Caslo, Lyngby, Denmark) emulsified 1:1 with complete Freund's adjuvant (Difco, Franklin Lakes, NJ) as previously described [13]. Immunization with the peptide was performed at days 0 and 7, following the *in-vivo* protocol timeline depicted in Figure 1. In the EAM model, immunization results in acute myocarditis that peaks ~21 days after immunization. Inflammation resolves slowly thereafter, whereas the number of cardiac fibroblasts progressively increases [15].

### Bone Marrow Macrophages Isolation

CD45.1-positive BALB/c mice (n=11) were used as donors to identify the transferred cells in the CD45.2 recipients. Briefly, femurs and tibiae were removed, the surrounding muscle tissue

was detached, and the bones were kept in Roswell Park Memorial Institute (RPMI) 1640 media. Marrow was flushed out with RPMI 1640 using a syringe and passed through a 70 µm nylon cell strainer (BD Biosciences) to remove debris. Cell suspensions were centrifuged and resuspended in complete RPMI 1640 medium supplemented with penicillin-streptomycin, 50 mM beta-mercaptoethanol, fetal bovine serum (FBS) and sodium pyruvate. Cells were seeded in 100 mm diameter low-adherent bacteriological petri dishes at 5 × $10^6$ cells per dish in 12 ml of complete RPMI medium containing L929 conditioned medium (30:20). Cells were cultured 7 days.

## BMM Labeling with 19F Nanoemulsion

BMM were labeled *in-vitro* with the $^{19}$F-based agent Cell Sense (CS-1000). Cell Sense is an aqueous colloidal suspension ("nanoemulsion") of PFC, having a total fluorine content of 145 mg/mL (Celsense Inc., Pittsburgh, PA, USA). The average nanoemulsion droplet size is 180 nm. It is formulated with excipients that facilitate entry of the PFC into all cell types, regardless of their ability to phagocytose. The PFC molecule used in Cell Sense is stable at low pH [1]. PFC was added to the cell culture medium at a concentration of 10 mg/mL and incubated for 18 h. After this incubation period, the cells were washed three times with phosphate buffered saline (PBS) (to eliminate free Cell Sense) and then counted after gentle harvesting with a cell scraper.

## *In-vitro* $^{19}$F-NMR Spectroscopy of Labeled Cells

In order to measure the mean $^{19}$F content present in the cells after labeling, quantitative $^{19}$F NMR measurements were performed in lysed cell pellets. A known number of labeled cells (~3 × $10^6$) were spun down and resuspended in 250 µl of 1% (v/v) Triton X-100 in PBS to lyse the cells. The cell lysate was mixed with 250 µl of a calibrated $^{19}$F reference solution, trifluoroacetic acid (TFA) at 0.1% v/v in D2O and placed in a 5 mm borosilicate NMR tube. The $^{19}$F NMR measurements were performed using a Bruker AVANCE III HD 400 MHz (9.4 T) NMR spectrometer equipped with a BBFO probe (Bruker BioSpin AG, Fällanden, Switzerland). The average $^{19}$F-fluorine content per cell was calculated from the ratio of the integrated areas of the TFA and PFC $^{19}$F spectra, normalized to the total cell number in the lysate. The PFC $^{19}$F spectra, acquired with 256 scans (32,000 points, 15 kHz spectral width and 5 s pre-acquisition delay) and processed with 5 Hz line broadening, contain several peaks, with the most prominent one located at -93 ppm. This peak was compared to TFA at -75 ppm for quantitative calculations.

## BMM Transfer into EAM Mice

PFC-labeled BMM (1 to 14 × $10^6$) suspended in 250 µl NaCl solution were injected IV into EAM mice either at day 20 or at day 9 (Figure 1).

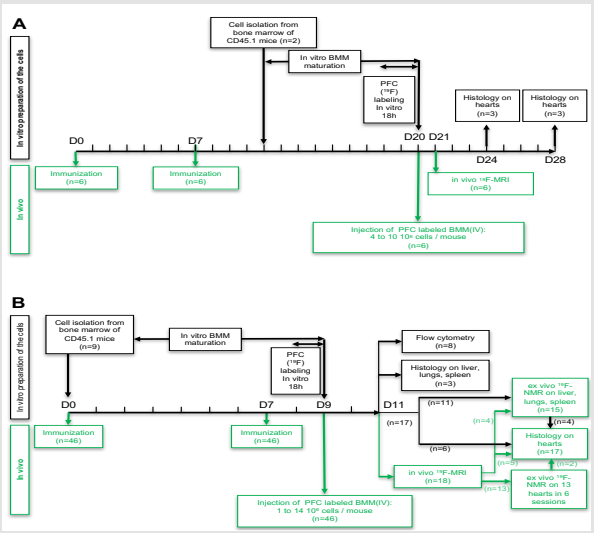


**Figure 1:** *In-vitro* and *in-vivo* protocol description. Overview of the time scale of the different experimental procedures. *In-vitro* procedures are depicted in black and *in-vivo* procedures are depicted in green.
(A) "Long time" protocol. *In-vitro*: Cell preparation. Bone marrow cells were isolated from femurs of CD45.1 mice (n=2) and cultured as described in the Materials and Methods section. *In-vivo*: At day 0
(D0) and D7, BALB/c mice (n=6) were immunized to induce EAM. At D20 the mice received an IV injection of $^{19}$F-labeled-BMM (from 4 to 10 × $10^6$ cells /mouse). All the mice were analyzed by in vivo 1H- and $^{19}$F-MRI at D21 and also either at D24 (n=3) or D28 (n=3). These mice were euthanized immediately after the MRI session and their hearts were analyzed by histology.

(B) "Short time" protocol. In-vitro: Cell preparation. At D0 bone marrow cells were isolated cultured as before (9 mice). In-vivo: At D0 and D7, BALB/c mice (n=46) were immunized as before. At D9 all the mice received an IV injection of $^{19}$F-labeled-BMM (from 2 to 10 × $10^6$ cells /mouse). Mice were scanned and / or analyzed 36 hours after BMM injection.

### $^{1}$H and $^{19}$F MRI

At day 11 (36 h post BMM injection), mice (n=18) were anesthetized with intraperitoneal injection of ketamine : medetomidine (75 mg/kg : 0.1 mg/kg). This anesthetic combination was chosen to avoid any $^{19}$F background signal from isoflurane, which accumulates in the fat pads of mice [23,24]. Body temperature was monitored with a rectal probe (SA Instruments, Stony Brook, NY) and kept constant at 37.0°C using tubing with circulating warm water. The animals were placed over a custom-designed 18-mm diameter quadrature surface coil tunable to both the $^{1}$H and $^{19}$F frequencies (400.2 and 376.6 MHz, respectively) [12]. Scanning was performed in a 31 cm horizontal-bore 9.4 T magnet (Magnex, Abingdon, UK) equipped with 400 mT/m gradient coils (Magnex, Abingdon, UK) and a VNMRS console (Varian, Palo Alto, USA).

For *in vivo* $^{19}$F-MRI, a stack of 3 to 5 prospective ECG-triggered short-axis $^{1}$H images of the heart was acquired with a gradient echo sequence (repetition time (TR) 11.1 ms, echo time (TE) 1.9 ms, signal averages 4, matrix 128×128, field of view 30×30 mm$^2$, slice thickness 2 mm, spectral width 78,125 Hz, total acquisition time ≈5 min). Next, a stack of non-triggered $^{19}$F images was acquired with the same view plan as the $^{1}$H images using a fast spin echo (TSE / RARE) sequence (TR 500 ms, TE 3.7 ms; echo-train length 4, signal averages 480, matrix 32x32, field of view 30×30mm$^2$, slice thickness 2 mm spectral width 156.25 kHz, total acquisition time 32 min). The $^{19}$F offset frequency was calibrated from unlocalized spectra (40 µs hard pulse, TR 1 s, 128 scans).

$^{19}$F images were processed in MATLAB with a 6-pixel Gaussian smoothing filter to reduce noise, then interpolated to match the background axis $^{1}$H image resolution and thresholded to display signals greater than 4-fold the standard deviation of the noise. Noise in the images was defined by selecting a 10 x 5 mm region in the field of view that did not cover the mouse body. $^{1}$H and $^{19}$F images corresponding to the same view plan were overlaid. In a subset of experiments (n=13), *ex vivo* $^{19}$F-MRS was performed on intact excised hearts placed in 1.8 ml microcentrifuge tubes filled with PBS buffer. One, two or four hearts in tubes were placed on the quadrature surface coil, and all hearts were scanned in 6 sessions with a pulse-acquire sequence (40 µs hard pulse, TR 1 s, 1024 or 2048 scans, spectral width 20161.3 Hz, 4129 points).

### Organ Collection

The mice were euthanized to collect the organs after MRI scanning. Thirteen of the hearts were immediately analyzed by $^{19}$F-MRS prior to being embedded in optimal cutting temperature (OCT) compound for immunohistochemistry. The liver, lungs, and spleen of 8 unscanned mice were also collected and divided for FACS analysis and immunohistochemistry, the latter set embedded in OCT; their bone marrow was also collected. The hearts of 10 other mice were also embedded in OCT. The liver, lungs, and spleen of 11 unscanned mice were collected for *ex-vivo* $^{19}$F NMR spectroscopic analysis.

### *Ex-vivo* $^{19}$F-NMR Spectroscopy of Excised Organs

The $^{19}$F NMR measurements were performed on the homogenates prepared from liver, lungs and spleen in 1% (v/v) Triton X-100 in PBS. The cell lysates were then mixed with 250 µl of 0.1% (v/v) TFA in D2O (calibrated $^{19}$F reference solution) and placed in a 5 mm borosilicate glass NMR tube. Spectra were acquired as described above in the "*In-vitro* $^{19}$F-NMR spectroscopy of labeled cells" section.

### Immunohistochemistry

OCT-embedded snap frozen tissues (heart, liver, lung and spleen) were sectioned in a cryostat at 6 µm thickness. Slides were air dried and fixed in acetone for 10 min at room temperature. Immunohistochemistry was performed on a Leica Bond Max according to the manufacturer's guidelines. The primary antibody, mouse anti-murine CD45.1-FITC (BD Cat. 553775, dilution 1:500), was linked with the secondary antibody, Rabbit anti-FITC (Serotec Cat. 4510-7804, dilution 1:500) and detected with Polymer anti-Rabbit AP-Refine-Kit (Cat. 9390) from Leica.

### Flow Cytometry

Single cell suspensions were prepared from bone marrow, liver, lungs and spleen using a cell strainer (70 µm) and RPMI medium for flow cytometry. After centrifugation, the pellets were resuspended in FACS buffer containing alexa647-conjugated anti-CD45.1 or IgG negative control for immunostaining (30 min at 4°C in the dark). Cells were washed with PBS and analyzed on a FACS LSRII (BD Biosciences, San Diego, CA) using BD FACS Diva software.

### Statistical Analyses

Values are given as mean ± standard deviation. Analyses of differences between groups were performed using one-way analysis of variance (ANOVA) with Bonferroni correction for multiple comparisons. Normality was evaluated with the Shapiro-Wilk test.

## Results

### *In-vitro* $^{19}$F-Labeling of BMM

The uptake after 18 hours of incubation with the PFC agent was quantified by $^{19}$F NMR and yielded 1.02 ± 0.50 × $10^{13}$ $^{19}$F atoms/cell (n=6). Cell viability was assayed immediately after labeling (18 h) by Trypan blue exclusion assay to evaluate the potential cytotoxicity due to labeling. The fraction of dead cells after PFC incubation was comparable to incubation in the absence of PFC (approximately 0.5% for both), indicating that the PFC agent safely labeled these cells *in-vitro* without significantly affecting their viability.

### Detection of $^{19}F$ Signal by $^{19}F$-MRI

Protocols with early (day 9) and late (day 20) $^{19}F$-labeled cell injection and cardiac follow-up $^{19}F$-MRI studies were applied (Figure 1). The late injection protocol followed a similar timeline as in our previous study where PFC was directly IV administered into EAM mice [12]. In 6 mice, PFC-labeled BMM were injected IV at day 20 after the first immunization of recipient mice, and *in-vivo* cardiac $^{19}F$-MRI was performed at days 21, 24 and 28. Under these conditions, no $^{19}F$-signals were detected in the heart by $^{19}F$-MRI (data not shown). Given that heart-infiltrating T cells and monocytes in the EAM model appear as early as 7-10 days after the first immunization, we decided to change the time course of our experiments. In the early series, $^{19}F$-labeled BMM were injected at day 9, and *in-vivo* cardiac $^{19}F$-MRI was performed at day 11. Although $^{19}F$ signal of variable intensity was detected in all animals by spectroscopy, the MRI signal detected in the heart was weak or absent (Figure 2A, arrowhead) and the majority of the $^{19}F$-signal was identified in the lungs (solid arrow) and the liver (dashed arrow).

These *in-vivo* data were confirmed by post-mortem analyses of the organs. Hearts were analyzed *ex-vivo* by $^{19}F$-MRS (n=13), and a faint spectral peak was detected within the combined cardiac tissue of 4 animals (Figure 2B). No $^{19}F$ *ex-vivo* heart signal was detected in the other animals. The $^{19}F$ content of the other organs (liver, lungs, spleen) was determined by $^{19}F$-NMR in tissue homogenates. Most of the organs analyzed contained variable amounts of $^{19}F$ (Figures 2C & 2D), reflecting the variable $^{19}F$-MRI signal seen *in vivo*. The fraction of $^{19}F$ recovered in the organs was significantly higher in the liver than the lungs ($p = 0.0096$, Figure 3), even though the liver $^{19}F$ content was below the limit of detection in two unscanned mice injected with weakly-labeled BMM ($6.49 \times 10^{11}$ and $2.37 \times 10^{11}$ $^{19}F$ atoms/cell).

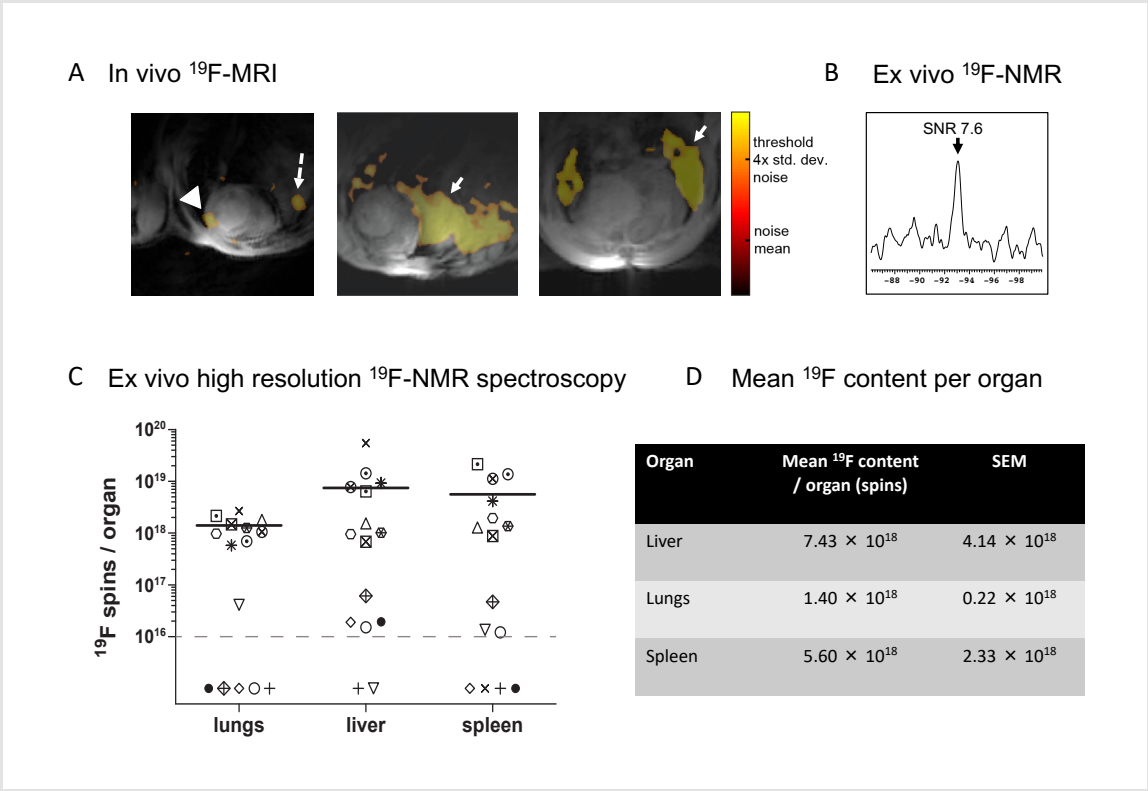


| Organ | Mean $^{19}F$ content / organ (spins) | SEM |
|---|---|---|
| Liver | $7.43 \times 10^{18}$ | $4.14 \times 10^{18}$ |
| Lungs | $1.40 \times 10^{18}$ | $0.22 \times 10^{18}$ |
| Spleen | $5.60 \times 10^{18}$ | $2.33 \times 10^{18}$ |

**Figure 2:** *In-vivo* and ex-vivo $^{19}F$-detection. (A) Representative in-vivo short-axis fused 19F and 1H images. 1H-signal appears in grey, 19F-signal in orange, and the heart, liver and lungs can clearly be identified. The highest signal was detected in the liver (dashed arrows) and in the lung (solid arrows). Heart signal is weak (arrowhead) and patchy, in agreement with a patchy infiltration of the EAM heart previously reported [12]. (B) Ex-vivo $^{19}F$-MRS of four intact hearts showing a PFC peak. (C) and (D) $^{19}F$ content in the liver, lungs and spleen determined by ex-vivo $^{19}F$-NMR spectroscopy of homogenate. (C) Each symbol corresponds to a different mouse; the black horizontal lines indicate the mean value for samples with signal. Samples without any $^{19}F$ signal appear below the dotted line indicating the limit of detection by $^{19}F$-NMR. (D) Table with the mean $^{19}F$-atom content per organ.

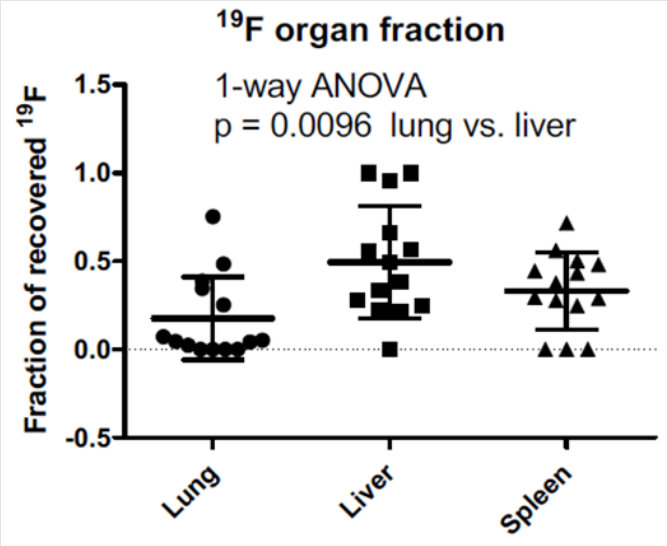


**Figure 3:** Fraction of recovered $^{19}F$ label in lungs, liver and spleen. The $^{19}F$ content of each organ is divided by the sum of the $^{19}F$ content of the three organs in a mouse. Samples with $^{19}F$ below the limit of detection by NMR were assigned the value of zero. The liver had on average the highest fraction of recovered $^{19}F$, which was significantly higher than the lung fraction.

## Immunohistochemistry

The presence of CD45.1 donor cell infiltrates was identified by immunohistochemistry in 12 out of 17 hearts, including 10 mice that underwent the same treatment but were not scanned. CD45.1 infiltrates were also found by immunohistochemistry in the liver, the lungs, and the spleen of the 3 mice analyzed (Figure 4).

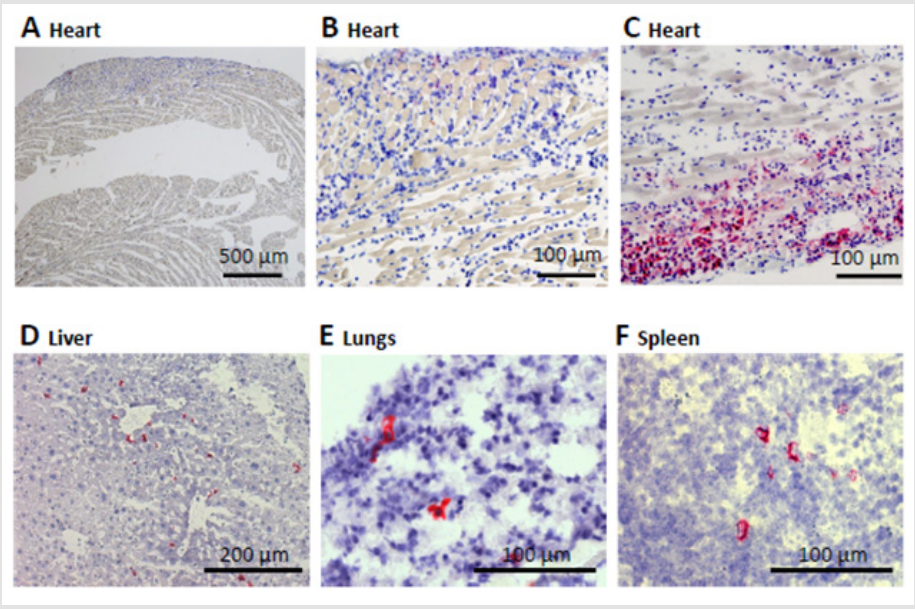


**Figure 4:** Immunohistochemistry CD45.1 in pink. ABC: Heart sections, D: Liver; E: Lungs; F: SpleenImmunohistological analysis of inflammatory cell infiltration. Representative CD45.1 staining to identify BMM donor cells (red, with blue hematoxylin staining of cell nuclei) in the CD45.2 recipients. (A) and (B) are representative examples of a heart with a low myocarditis score (1) and no cardiac infiltration by donor BMM cells. (C) illustrates weak cardiac infiltration by donor BMM cells in a heart with myocarditis score of 2. The mice in (A, B and C) were injected with the same labeled BMM preparation. CD45.1 positive infiltrates can be observed in liver (D), lungs (E), and spleen (F) sections. The scale is indicated on each image.

### Flow Cytometry

To confirm the immunohistochemistry results, flow cytometry of the CD45.1 marker was used to follow the distribution of the donor BMM in the different organs (Figure 5). Flow cytometric analysis confirmed the presence of the injected CD45.1 cells in the organs, including bone marrow (6.2 ± 0.2 % of the gated cells), spleen (0.4 ± 0.03 %), liver (0.2 ± 0.04 %) and lungs (0.4 ± 0.2 %).

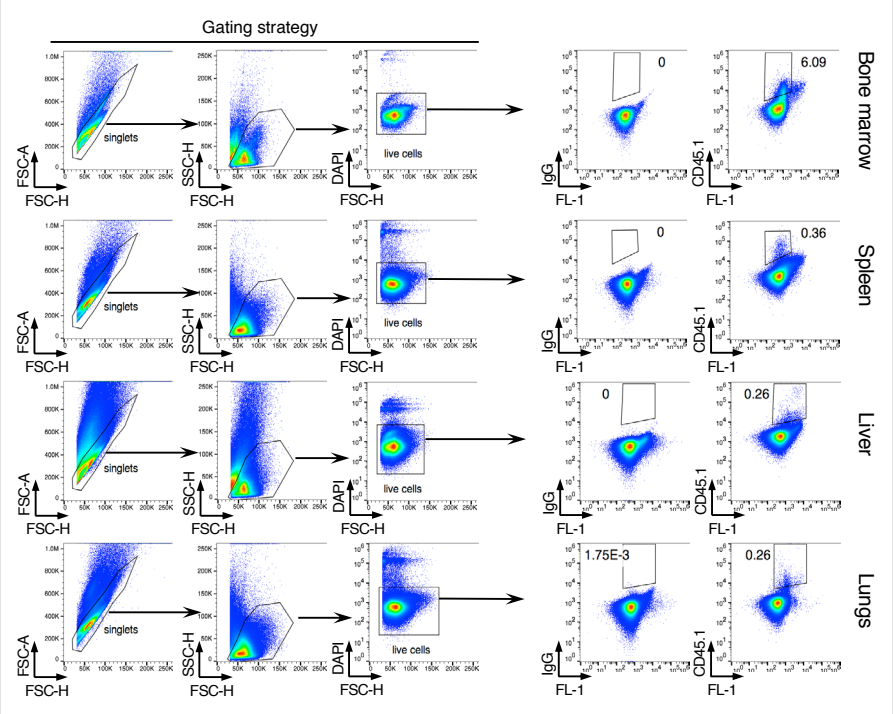


**Figure 5:** Flow cytometry analysis. Cells were isolated from the indicated organs and analyzed by flow cytometry. Arrows in the left panel indicate gating strategy. Plots in the right panel show CD45.1 analysis on gated populations. Isotype IgG were used as negative control. FL-1 represents empty channel. Numbers indicate percentage of cells in the adjacent gates. Data are representative of 8 mice.

## Discussion

The main findings of the current study can be summarized as follows: 1) BMM were successfully labeled *in-vitro* by PFC, yielding (1.02 ± 0.50) x $10^{13}$ $^{19}$F atoms/cell while preserving their viability. 2) As a proof-of-concept, IV-injected $^{19}$F-labeled mature BMM can be tracked in the EAM model by $^{19}$F-MRI, demonstrating their accumulation primarily in the liver, spleen and lungs, while accumulation in the inflamed myocardium is minimal despite the development of myocarditis. 3) The distribution of $^{19}$F-labeled BMM revealed by *in-vivo* $^{19}$F-MRI was confirmed by *ex-vivo* $^{19}$F-NMR spectroscopy, immunohistology, and flow cytometry.

### Detectable Migration of IV-Injected BMM into Extra-Cardiac Tissue

The presence of the PFC-labeled BMM in the liver, lungs, and spleen was readily apparent by $^{19}$F-MRI and confirmed by *ex-vivo* $^{19}$F-NMR spectroscopy. This pattern of accumulation is reminiscent of the one previously reported for labeled BMM tracked by single-photon emission computed tomography (SPECT) and $T_2$*-weighted MRI, where the cells were primarily located in the liver and spleen after initially being found mainly in the lung [25]. The similar pattern suggests that these two different labeling methods do not affect the BMM migration behavior, but a functional effect due to the labeling cannot be ruled out.

### Weak Invasion of the Myocardium in the EAM Model by BBM

In earlier studies, direct IV injection of PFC nanoemulsions successfully labeled macrophages in inflamed myocardium of the EAM model [12] and in other models of myocarditis [26]. In the current study, however, PFC-labeled BMM, when injected IV, did not migrate to the site of inflammation in the heart at a high level and were rarely detectable there by *in-vivo* $^{19}$F-MRI or *ex-vivo* $^{19}$F-NMR spectroscopy. *In-vivo* $^{19}$F-MRI and *ex-vivo* $^{19}$F-NMR spectroscopy detected a $^{19}$F signal in the heart in 2 out of 18 and 1 out of 6 experiments, respectively. However, *in-vivo* and *ex-vivo* signals were not detected in the same mice, and the apparent *in-vivo* $^{19}$F cardiac signal may be due to partial-volume effects from the neighboring lung and liver. In an earlier study [18], the same *in-vivo* $^{19}$F-MRI experimental setup yielded a threshold for detection of 1.5 × $10^{17}$

$^{19}$F-atoms per 0.63mm$^3$, which translates to approximately 8500 cells/µl (assuming a labeling of $10^{13}$ $^{19}$F-atoms/cell) with the 1.76 mm$^3$ voxel size used here. Nonetheless, a substantial fraction of the injected labeled cells - on the order of 1% or more - would have to be concentrated in a 9 mm$^3$ volume (assuming five adjacent voxels) of the myocardium in order to be reliably detected.

This may partially explain the infrequent and inconsistent detection of myocardial $^{19}$F signal despite the presence of CD45.1-positive transferred cells in the myocardium two-thirds of the time (i.e. in 12 out of 17 hearts by immunohistology). In the case where a $^{19}$F signal was detected *ex vivo* (Figure 2B), the signal is estimated to correspond to ~2 x $10^{17}$ $^{19}$F atoms, assuming the same coil loading and spatial distribution of $^{19}$F in the phantom used for calibration and was likely to diffuse to be detectable by imaging. A number of factors must be considered regarding the origin and fate of PFC-labeled macrophages in the EAM mouse heart in the interpretation of these results. Depending on the particular model used, there is evidence for both local macrophage differentiation or proliferation in the inflamed myocardium [27-29] and also macrophages derived from recruited blood monocytes [30].

Reports from our laboratories clearly indicate an important role of heart-infiltrating bone-marrow-derived CD133-expressing immature monocyte-like precursor cells as a potential source of both myofibroblasts and macrophages in the inflamed heart [28,31,32]. On the one hand, the uptake of IV-infused PFC by phagocytic cells in the circulation, followed by their migration to the inflamed myocardium, provides a good rationale for the myocardial accumulation of the $^{19}$F signal in previous myocarditis studies [12, 26]. Bönner et al. have shown the ability of blood-derived leukocytes to take up PFC [33], which would support this route of myocardial PFC entry. On the other hand, it is possible for cells already present in the heart to take up infused PFC in quantities sufficient to be imaged. For example, Ding et al. demonstrated infiltration of the inflamed myocardium in an ischemia-reperfusion model not only by blood-derived monocytes but also by epicardium-derived cells (EPDC) [34].

These EPDC displayed strong endocytic activity to take up the IV-injected PFC emulsion and infiltrated the inflamed myocardium in a time-dependent manner, such that they represented the main source of $^{19}$F-labeled cells 3 days after the ischemia-reperfusion event. If BMM migration is not affected by labeling, the present results would indicate that the injected BMM are unable to effectively infiltrate the heart in large numbers. This would be consistent with the view that accumulation of macrophages within the inflamed heart results either from differentiation of recruited or resident precursor cells or from proliferation of those already present. Nevertheless, to better test this mechanism of PFC accumulation in the inflamed myocardium would require a separate protocol to track PFC-labeled monocytes in the murine EAM model.

## Limitations

The techniques used in this study result in a number of limitations. One important limitation of the PFC-labeling technique is the considerable variability of the achieved loading, ranging from 2.37 × $10^{11}$ to 5.34 × $10^{13}$ $^{19}$F-atoms/cell, which translated into the variable number of injected BMM cells, ranging from 1 to 14 × $10^6$ per animal. Overall, less $^{19}$F was administered to the mice as PFC-labeled BMMs than in our previous myocarditis study with infused PFC, and this may limit sensitivity. Despite the >10-fold higher average per-cell $^{19}$F content compared to prior studies using IV-transferred PFC-labeled cells [18,20], there still was not sufficient sensitivity to detect the label in the target tissue *in vivo*. Additionally, the *in vivo* MRI and *ex vivo* MRS were performed with a surface coil, which provides high sensitivity but makes absolute quantitation of the $^{19}$F more difficult. To better quantitate the *in vivo* $^{19}$F signal, a volume coil could be used with a reference standard in the field of view.

The sensitivity of the $^{19}$F imaging sequence could also be further improved with a lower acquisition bandwidth, or by using a spoiled-gradient echo (SPGR), steady state at free precession (SSFP)-type method instead [21]. Although the procedure to differentiate bone-marrow derived macrophage precursor cells with L929-conditioned medium is a well-accepted method to generate a relatively uniform population of mature quiescent BMM in high yield [35], the phenotype of the transferred cells found in the liver, lungs, spleen, heart and bone marrow was not characterized beyond the presence of the CD45.1 marker. While PFC labeling did not affect BMM pre-infusion viability, further study is needed to understand whether it has any effect on cell migration to the inflamed myocardium in the EAM model.

## Conclusion

BMM were successfully labeled *in-vitro* with PFC and tracked *in-vivo* by non-invasive $^{19}$F-MRI. In the EAM model, non-invasive $^{19}$F-MRI reliably demonstrates accumulation of IV-injected mature BMM primarily in the liver, spleen, and lungs, with little migration to the inflamed myocardium. Thus, this technique has the potential to non-invasively track the *in-vivo* migration of specific cell types in the EAM model. These findings suggest that either resident inflammatory cells, macrophages differentiating from heart-infiltrating immature precursors represent the main source of differentiated macrophages accumulating in the heart in myocarditis and point the way to further studies that directly address these questions.

## Declarations

### Ethics Approval and Consent to Participate

All animal procedures were approved by the institutional ethics committee and performed in accordance with an authorization for

animal experimentation issued by the local regulatory agency: le Service de la Consommation et des Affaires vétérinaires du Canton de Vaud (SCAV, Epalinges, Switzerland).

### Consent for Publication

Not applicable.

### Availability of Data and Materials

The datasets used and analyzed during the current study are available from the corresponding author (J.S.) on reasonable request.

### Competing Interests

The authors declare that they have no competing interests.

### Funding

This work was supported by the Swiss National Science Foundation grants 310030_163050 and PZ00P3_154719, as well as a grant from the Swiss Heart Foundation to J.S. (2015).

## Authors' Contributions

**Study Conception and Design:** Gonzales, Schwitter, Helm, Eriksson

**Acquisition of Data:** Gonzales, Yoshihara, van Heeswijk, Mieville, Blyszczuk, Kania

**Analysis and Interpretation of Data:** Gonzales, Yoshihara, Mieville, Blyszczuk, Kania

**Drafting of Manuscript:** Gonzales, Yoshihara, Schwitter, Eriksson

**Critical Revision:** van Heeswijk, Blyszczuk

## Acknowledgment

We are grateful to Carola J. Romero, Corina M. Berset, Anne-Catherine Clerc for their technical assistance.

## References

1. Ahrens ET, Flores R, Xu H, Morel PA (2005) *In vivo* imaging platform for tracking immunotherapeutic cells. Nat Biotechnol 23(8): 983-987.
2. Schwitter J (2008) Extending the frontiers of cardiac magnetic resonance. Circulation 118(2): 109-112.
3. Kadayakkara DK, Beatty PL, Turner MS, Janjic JM, Ahrens ET, et al. (2010) Inflammation driven by overexpression of the hypoglycosylated abnormal mucin 1 (MUC1) links inflammatory bowel disease and pancreatitis. Pancreas 39(4): 510-515.
4. Srinivas M, Turner MS, Janjic JM, Morel PA, Laidlaw DH, et al. (2009) *In vivo* cytometry of antigen-specific t cells using $^{19}$F MRI. Magn Reson Med 62(3): 747-753.
5. Ramos IT, Henningsson M, Nezafat M, Lavin B, Lorrio S, et al. (2018) Simultaneous assessment of cardiac inflammation and extracellular matrix remodeling after myocardial infarction. Circ Cardiovasc Imaging 11(11): e007453.
6. Flögel U, Ding Z, Hardung H, Jander S, Reichmann G, et al. (2008) *In vivo* monitoring of inflammation after cardiac and cerebral ischemia by fluorine magnetic resonance imaging. Circulation 118(2): 140-148.
7. Ye YX, Basse Lüsebrink TC, Arias Loza PA, Kocoski V, Kampf T, et al. (2013) Monitoring of monocyte recruitment in reperfused myocardial infarction with intramyocardial hemorrhage and microvascular obstruction by combined fluorine 19 and proton cardiac magnetic resonance imaging. Circulation 128(17): 1878-1888.
8. Ebner B, Behm P, Jacoby C, Burghoff S, French BA, et al. (2010) Early assessment of pulmonary inflammation by $^{19}$F MRI *in vivo*. Circ Cardiovasc Imaging 3(2): 202-210.
9. van Heeswijk RB, Pellegrin M, Flögel U, Gonzales C, Aubert JF, et al. (2015) Fluorine MR imaging of inflammation in atherosclerotic plaque *in vivo*. Radiology 275(2): 421-429.
10. Flögel U, Burghoff S, van Lent PLEM, Temme S, Galbarz L, et al. (2012) Selective activation of adenosine A2A receptors on immune cells by a CD73-dependent prodrug suppresses joint inflammation in experimental rheumatoid arthritis. Science Translational Medicine 4(146): 146ra108.
11. Balducci A, Wen Y, Zhang Y, Helfer BM, Hitchens TK, et al. (2013) A novel probe for the non-invasive detection of tumor-associated inflammation. Oncoimmunology 2(2): e23034.
12. van Heeswijk RB, De Blois J, Kania G, Gonzales C, Blyszczuk P, et al. (2013) Selective *in vivo* visualization of immune-cell infiltration in a mouse model of autoimmune myocarditis by fluorine-19 cardiac magnetic resonance. Circ Cardiovasc Imaging 6(2): 277-284.
13. Eriksson U, Ricci R, Hunziker L, Kurrer MO, Oudit GY, et al. (2003) Dendritic cell-induced autoimmune heart failure requires cooperation between adaptive and innate immunity. Nat Med 9(12): 1484-1490.
14. Heymans S, Eriksson U, Lehtonen J, Cooper LT (2016) The quest for new approaches in myocarditis and inflammatory cardiomyopathy. J Am Coll Cardiol 68(21): 2348-2364.
15. Blyszczuk P, Kania G, Dieterle T, Marty RR, Valaperti A, et al. (2009) Myeloid differentiation factor-88/interleukin-1 signaling controls cardiac fibrosis and heart failure progression in inflammatory dilated cardiomyopathy. Circ Res 105(9): 912-920.
16. Kania G, Blyszczuk P, Valaperti A, Dieterle T, Leimenstoll B, et al. (2008) Prominin-1+/CD133+ bone marrow-derived heart-resident cells suppress experimental autoimmune myocarditis. Cardiovasc Res 80(2): 236-245.
17. Valaperti A, Marty RR, Kania G, Germano D, Mauermann N, et al. (2008) CD11b(+) monocytes abrogate th17 CD4(+) T cell-mediated experimental autoimmune myocarditis. J Immunol 180(4): 2686-2695.
18. Gonzales C, Yoshihara HAI, Dilek N, Leignadier J, Irving M, et al. (2016) In-Vivo detection and tracking of T cells in various organs in a melanoma tumor model by $^{19}$F-fluorine MRS/MRI. PloS One 11(10): e0164557.
19. Gaudet JM, Ribot EJ, Chen Y, Gilbert KM, Foster PJ (2015) Tracking the fate of stem cell implants with fluorine-19 MRI. PloS One 10(3): e0118544.
20. Chapelin F, Gao S, Okada H, Weber TG, Messer K, et al. (2017) Fluorine-19 nuclear magnetic resonance of chimeric antigen receptor T cell biodistribution in murine cancer model. Sci Rep 7: 17748.
21. Constantinides C, Maguire M, McNeill E, Carnicer R, Swider E, et al. (2018) Fast, quantitative, murine cardiac $^{19}$F MRI/MRS of PFCE-labeled progenitor stem cells and macrophages at 9.4T. PloS One 13(1): e0190558.
22. Gomes RSM, Neves RPD, Cochlin L, Lima A, Carvalho R, et al. (2013) Efficient Pro-survival/angiogenic miRNA Delivery by an MRI-Detectable Nanomaterial. ACS Nano 7(4): 3362-3372.

23. Eger EI, Saidman LJ (2005) Illustrations of inhaled anesthetic uptake, including intertissue diffusion to and from fat. Anesth Analg 100(4): 1020-1033.

24. Constantinides C, Maguire ML, Stork L, Swider E, Srinivas M, et al. (2017) Temporal accumulation and localization of isoflurane in the C57BL/6 mouse and assessment of its potential contamination in 19 F MRI with perfluoro-crown-ether-labeled cardiac progenitor cells at 9.4 Tesla. J Magn Reson Imaging 45(6): 1659-1667.

25. Gorantla S, Dou H, Boska M, Destache CJ, Nelson J, et al. (2006) Quantitative magnetic resonance and SPECT imaging for macrophage tissue migration and nanoformulated drug delivery. J Leukoc Biol 80(5): 1165-1174.

26. Jacoby C, Borg N, Heusch P, Sauter M, Bönner F, et al. (2014) Visualization of immune cell infiltration in experimental viral myocarditis by (19)F MRI *in vivo*. Magn Reson Mater Phy 27(1): 101-106.

27. Blyszczuk P, Behnke S, Lüscher TF, Eriksson U, Kania G (2013) GM-CSF promotes inflammatory dendritic cell formation but does not contribute to disease progression in experimental autoimmune myocarditis. Biochim Biophys Acta 1833(4): 934-944.

28. Kania G, Blyszczuk P, Stein S, Valaperti A, Germano D, et al. (2009) Heart-infiltrating prominin-1+/CD133+ progenitor cells represent the cellular source of transforming growth factor beta-mediated cardiac fibrosis in experimental autoimmune myocarditis. Circ Res 105(5): 462-470.

29. Epelman S, Lavine KJ, Beaudin AE, Sojka DK, Carrero JA, et al. (2014) Embryonic and adult-derived resident cardiac macrophages are maintained through distinct mechanisms at steady state and during inflammation. Immunity 40(1): 91-104.

30. Leuschner F, Rauch PJ, Ueno T, Gorbatov R, Marinelli B, et al. (2012) Rapid monocyte kinetics in acute myocardial infarction are sustained by extramedullary monocytopoiesis. J Exp Med 209(1): 123-137.

31. Blyszczuk P, Berthonneche C, Behnke S, Glönkler M, Moch H, et al. (2013) Nitric oxide synthase 2 is required for conversion of pro-fibrogenic inflammatory CD133(+) progenitors into F4/80(+) macrophages in experimental autoimmune myocarditis. Cardiovasc Res 97(2): 219-229.

32. Kania G, Blyszczuk P, Eriksson U (2009) Mechanisms of cardiac fibrosis in inflammatory heart disease. Trends Cardiovasc Med 19(8): 247-252.

33. Bönner F, Merx MW, Klingel K, Begovatz P, Flögel U, et al. (2015) Monocyte imaging after myocardial infarction with $^{19}$F MRI at 3 T: a pilot study in explanted porcine hearts. European Heart Journal - Cardiovascular Imaging 16(6): 612-620.

34. Ding Z, Temme S, Quast C, Friebe D, Jacoby C, et al. (2016) Epicardium-derived cells formed after myocardial injury display phagocytic activity permitting *in vivo* labeling and tracking. Stem Cells Transl Med 5(5): 639-650.

35. Zhang X, Goncalves R, Mosser DM (2008) The isolation and characterization of murine macrophages. Curr Protoc Immunol Chapter 14: Unit 14.1.

ISSN: 2574-1241

DOI: 10.26717/BJSTR.2020.29.004798

**Juerg Schwitter**. Biomed J Sci & Tech Res